



## Velocity gradient induced line splitting in x-ray emission accompanying plasma–wall interaction



M. Šmíd<sup>a,b,\*</sup>, O. Renner<sup>a</sup>, R. Liska<sup>b</sup>

<sup>a</sup> Institute of Physics, Academy of Sciences, Na Slovance 2, Prague 8, 182 21, Czech Republic

<sup>b</sup> Czech Technical University in Prague, FNSPE, Brehova 7, Prague 1, 115 19, Czech Republic

### ARTICLE INFO

#### Article history:

Received 15 January 2013

Received in revised form

5 March 2013

Accepted 9 April 2013

Available online 18 April 2013

#### Keywords:

Laser-produced plasmas

X-ray spectroscopy

Plasma–wall interaction

Spectral line profiles

Doppler shift

Ion velocity gradients

### ABSTRACT

High-resolution x-ray spectroscopy was applied to study the ion back-scattering in plasma–wall interaction. In experiments carried out on the Prague Asterix Laser System (PALS), the energetic ions produced at thin laser burnt-through Al foil impacted the secondary C target where they were decelerated, trapped and scattered in radial and backward directions. The environmental conditions in near-wall plasmas were analyzed using the high-dispersion x-ray spectroscopy and temporally-resolved x-ray imaging. The radial expansion of ions back-scattered in the near-wall region was directly observed via the Doppler effect induced splitting of the Al He $\alpha$  intercombination line. The experimentally observed line splitting was modeled using a combination of the 2D arbitrary Lagrangian Eulerian hydrodynamics code PALE with the multifluid code MULTIF and spectrally postprocessed using HULLAC atomic model builder and CRETIN collisional-radiative code.

© 2013 Elsevier Ltd. All rights reserved.

### 1. Introduction

Forming and propagation of collimated plasma jets including their interaction with surrounding media are systematically investigated in two diverse scientific disciplines. Benefiting from the existence of high-energy-density facilities (in particular, high power lasers, fast Z-pinches and other pulsed power devices), processes occurring in extreme astrophysical conditions can be either directly studied in the laboratory [1] or rescaled with respect to several types of scaling laws [2]. In the fusion related research, the energetic particle jets offer alternate possibilities for realization of the inertial confinement fusion [3,4]. Further fusion-relevant applications relate to studies of the material erosion and migration at plasma facing components, particularly in context with the

search for novel inner-wall materials of fusion devices [5,6]. Optimization of these plasma-exposed materials is conditioned by a detailed understanding of transient processes accompanying interaction of intense fluxes of charged particles with solids (generally known as plasma–wall interaction, PWI).

Mechanisms of the energy transfer to solid surfaces include ion deceleration and stopping in the near-wall region, shock wave generation, formation of highly excited Rydberg states or hollow atoms with multiple inner vacancies, charge transfer processes, and ion neutralization. A brief survey of these processes and relevant PWI scenarios can be found (e.g., in paper [7] and references therein).

The purpose of this article is to contribute to the x-ray spectroscopic characterization of environmental conditions at solid targets exposed to directional flows of energetic particles, concretely to the fast ions deceleration, stopping, and back-scattering in the near-wall plasma region. Recent experiments directed to the investigation of the ions trapping and thermalization in the near-wall

\* Corresponding author at: Institute of Physics, Academy of Sciences, Na Slovance 2, Prague 8, 182 21, Czech Republic. Tel.: +420 266052136.  
E-mail address: [smidm@fzu.cz](mailto:smidm@fzu.cz) (M. Šmíd).

colliding plasmas revealed either monotonic deceleration of the plasma jets launched from the single-side laser-exploded Al foils and impinging onto the secondary Mg targets [8] or oscillations in the velocity profiles of the Al ions produced at the double-side laser-irradiated Al/Mg targets [9]. In both these experiments, the deceleration profiles of the Al ions incident onto the Mg surface were quantitatively characterized via Doppler shifts observed in emission of the optically thin J-satellite from the hydrogenic Al Ly $\alpha$  spectral group.

Here we report the x-ray spectroscopic investigation of the plasma-wall interaction at single-side laser-irradiated double-foil Al/C targets. In contrast to previous experiments, the PWI was studied using the characteristic line emission of the He-like Al ions. The spatially resolved, time-integrated Al He $\alpha$  spectra measured using a high-dispersion x-ray spectrometer reveal a distinct line splitting which was interpreted in terms of the Doppler effect induced line shifts due to the high velocity gradients of the Al ions back-scattered from the secondary C target. Following the procedure suggested by Wark et al. [10] for modeling of the spectral emission from plasmas with large velocity gradients, we have performed extensive quasi-2D multifluid hydrodynamic simulations which were post-processed with a radiative transfer routine to construct the synthetic spectra. Their comparison with the experimental data confirm the validity of the suggested line splitting mechanism, i.e., the effect connected with the velocity gradients in the back-streaming Al ions. This first precise x-ray observation of the ions back-scattering at plasma-exposed solid targets provides the application-important data necessary to a development of new-generation plasma facing components and, in the same time, reliable input for benchmarking the complex computer simulations of hot dense laser-produced plasmas.

## 2. Experiment

The experiment was performed on the iodine laser system of the PALS Research Centre in Prague [11]. The targets consisted alternately of a single Al foil or two parallel foils of Al (purity 99.1%, thickness 0.8  $\mu\text{m}$ ) and C (250- $\mu\text{m}$ -thick pyrolytic graphite) interleaved by a distance of 600  $\mu\text{m}$ , as schematically shown in Fig. 1. The laser beam delivering 27 J of frequency-tripled radiation

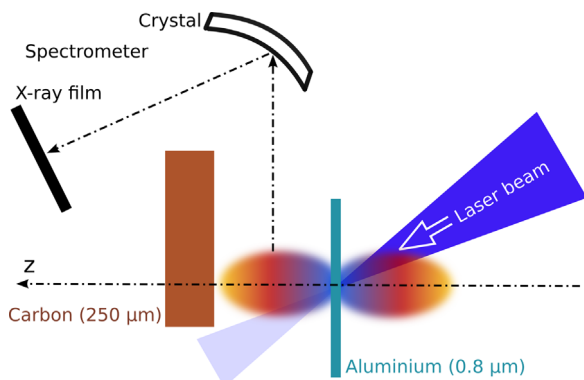


Fig. 1. Experimental setup.

(438 nm) in a pulse length of 0.27 ns (full width at half maximum) and a flux intensity of  $1.5 \times 10^{15}$  W/cm $^2$  was incident onto the primary, jet-producing Al target at an angle inclined by 30° from its normal. The reason for the oblique incidence of the laser beam onto the Al foil follows from modeling of the jets formation in transmission geometry performed by the Prague Arbitrary Lagrangian Eulerian hydrocode PALE [12]. The simulations demonstrate that the Al foil burns through before the laser pulse maximum. When applying the oblique laser incidence, the beam does not hit the secondary target and the plasma jet launched in a direction of the normal to the Al foil surface interacts with the unperturbed target, thus creating a well characterized environment for PWI studies.

The standard diagnostic complex used for the PWI investigation at PALS has already been described in paper [7]. Here we concentrate to results obtained using the principal diagnostics, the vertical-geometry Johann spectrometer (VJS) [13]. This instrument equipped with the cylindrically bent crystal of quartz (100) provides simultaneously two mirror-symmetric sets of 1D spatially resolved spectra with the spectral resolution  $\lambda/\Delta\lambda=6000$  and the spatial resolution 5  $\mu\text{m}$  along the experimental axis (denoted as  $z$ ). The spectra were observed in the direction parallel to the Al target surface and covered the wavelength range 7.73–7.89 Å including the He $\alpha$  resonance (He $\alpha$  w,  $1s2p\ ^1P_1 \rightarrow 1s^2\ ^1S_0$  transition at 7.757 Å) and intercombination (He $\alpha$  y,  $1s2p\ ^3P_1 \rightarrow 1s^2\ ^1S_0$ , 7.807 Å) lines and their Li-like satellites.

The spectra recorded at single Al and double foil Al/C targets are shown in Fig. 2. The spatial resolution is obtained along the  $z$ -axis, the laser irradiates the Al target from above. At both types of targets, the strongest line emission is observed near the Al foil surface ( $z=0\ \mu\text{m}$ ). Above the front (irradiated) side of the Al target, the  $w$  and  $y$  lines are well visible up to the distance of about 400 and 700  $\mu\text{m}$ , respectively, and the satellites emission is obscured by non-ablated parts of the Al foil. At the rear side of the single foil target (see Fig. 2a), the spatial extent of the  $w$  and  $y$  line emission is about 350  $\mu\text{m}$  and the satellites are restricted to the region of about 80  $\mu\text{m}$ . Most of the satellites emitted in the wavelength range of 7.85–7.88 Å originate from  $1s\ 2p^2 \rightarrow 1s^2\ 2p$  transitions but they can also be present at wings of the intercombination (transitions  $1s\ 2p\ 2s \rightarrow 1s^2\ 2s$ ) and the resonance line ( $1s\ 2p\ 3l \rightarrow 1s^2\ 3l$ ).

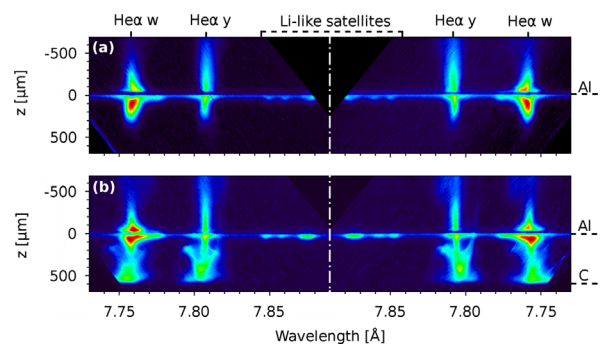


Fig. 2. Spatially resolved spectra of Al He $\alpha$  group observed at laser-exploded single Al (a) and double foil Al/C (b) targets.

As shown in Fig. 2b, the character of the spectra recorded at Al/C targets is considerably different. The  $w$  and  $y$  spectral lines are visible throughout the inter-foil space, they are considerably broadened and split in dependence on the distance from the secondary target. These characteristic features bear on the plasma evolution: the jet launched from the rear side of the Al foil strikes the secondary target positioned at the distance  $z=600\ \mu\text{m}$ , the Al ions are decelerated, trapped and back-scattered from the C surface [9]. The region of the enhanced line emission close to the C foil relates to the strongly collisional plasma produced by interaction of the impinging and counter-propagating ions (composed of the back-scattered Al ions and C ions ejected from the secondary target). The increased density of the near-wall plasma explains in combination with the opacity effects and satellites production the significant broadening of the observed spectral profiles (particularly distinct for the resonance line).

This scenario is validated by a time-resolved record from the pinhole coupled to the low-magnification x-ray streak camera. The streak image presented in Fig. 3 demonstrates the strong x-ray emission from the Al foil which burns through well before the laser pulse maximum (corresponding to time  $t=0$  ns). Much weaker x-ray emission observed close to the secondary target indicates the impact of outflowing Al ions onto the C surface starting from  $t\approx 0.5$  ns, their collision with the gradually evolving near-wall plasma and back-scattering toward the non-ablated Al foil.

Hereafter we shall concentrate to the interpretation of the spectral line splitting which is well visible in  $w$  and  $y$  profiles. These lines and particularly the ratio  $\alpha=I_w/I_y$  of their integrated intensities  $I_{w,y}$  were often used for diagnostic purposes. In equilibrium plasmas, the upper states of both lines are populated via the electron impact excitation from the  $1s^2$  level and by a collisional transfer between the fine structure of the  $1s2l$  levels. For high electron densities, population is essentially transferred from the triplet to the singlet levels resulting in relatively high values of  $\alpha$  ratios ( $\alpha=1-5$ ) depending on the plasma density [14].

However, a more complicated situation occurs in non-stationary super-cooled plasmas, where the population of H- and He-like ions does not correspond to the equilibrium condition. Here the relative population of H-like

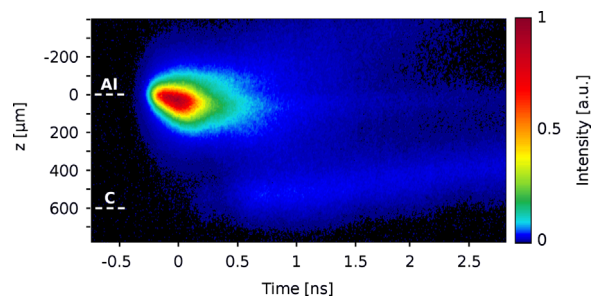


**Fig. 3.** Streak camera record of X-ray emission from Al/C target. Plasma created at Al foil ( $z=0$ ) strikes the secondary C target ( $z=600\ \mu\text{m}$ ) at  $t\approx 0.5$  ns, afterwards the plasma cloud moves backwards toward the primary Al target.

species may be much higher and the recombination process from the  $1s$  state becomes the dominant mechanism in populating the  $1s2p$  states. Since the recombination populates both upper states with the ratio  $1/3$  related to their statistical weights, the  $\alpha$  may also decrease down to this value.

In our experiment, as well as in several other laser-plasma experiments (e.g., [15,16]), the  $\alpha$  ratio is quite high ( $> 2$ ) near the irradiated foil but approaches unity or even drops below it with the increasing distance from the foil, thus showing that the recombination processes starts to dominate. Consequently, the use of the  $\alpha$  ratio for a simple evaluation of the temperature and density is questionable, as it depends not only on the current plasma parameters, but also on their history.

Concerning the diagnostic applications of individual  $w$  and  $y$  profiles, the optical depth  $\tau$  of the dominant resonance line is generally large. For instance, the realistic estimates of the plasma size  $L=100\ \mu\text{m}$ , temperature  $T=500$  eV and density  $\rho=0.001\ \text{g/cm}^3$  inserted into the collisional-radiative code PrismSPECT [17] provide a value of  $\tau > 5$ . Consequently, this line is very sensitive to the radiation transport effects and therefore difficult to evaluate. On the other hand, the optical depth of the inter-combination line is much lower, thus providing excellent possibilities for the observation of velocity profiles via Doppler shifts, i.e., high intensity over the whole observed region and low reabsorption.

### 3. Computer modeling

In order to simulate the observed line-profiles, a two dimensional multifluid model with spectral output is needed. This model was created by combining four codes into a system depicted in Fig. 4.

PALE [12] is the arbitrary Lagrangian–Eulerian hydrodynamic code which calculated the laser absorption at the Al foil and its consequent expansion on a 2D Lagrangian mesh in a cylindrical geometry. This code does not handle the plasma interpenetration, therefore the simulation stops at instant when the Al plasma reaches the C target ( $t=0.3$  ns). In this stage, the hydrodynamic parameters are passed to MULTIF hydrodynamic code [18] as initial conditions for further modeling. This code runs a two fluid (Al/C) simulation with interaction terms between the plasma species obtained by means of moments of the Fokker–Planck equation. Since MULTIF is a 1D code, a pseudo-2D regime has been formed: The Lagrangian data from PALE have been interpolated on a rectangular Eulerian grid and each axial cut of this grid was passed to separate MULTIF calculation. Consequently, seven Multif simulations have been performed, each one for a fixed radius  $r=0, 40, 80, 120, 160, 200,$  and  $240\ \mu\text{m}$ . For the spectral postprocessing, the output from PALE and from the set of MULTIF runs have been interpolated on a smooth 2D Eulerian grid.

The HULLAC [19] atomic model builder calculates detailed atomic data needed for the collisional-radiative spectral simulation, specifically tailored to include all necessary levels and transitions. The Al model includes levels of H-like ( $1s-7l$ ), He-like ( $1s^2-1s\ 6l, 2l^2-2l\ 4l, 3l^2, 3l\ 4l$ ), Li-like ( $1s^2\ 2l, 1s^2\ 3l, 1s\ 2l^2, 1s\ 2l\ 3l$ ), and Be-like ( $1s^2\ 2l^2$ )

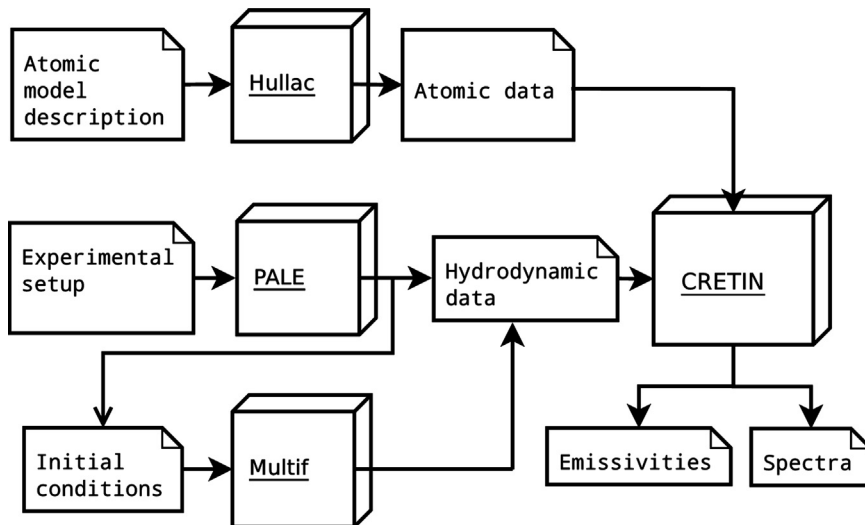


Fig. 4. Interconnection of the atomic, hydrodynamic and collisional-radiative codes used in the simulation.

atoms. Finally, CRETIN collisional-radiative solver [20] reads hydrodynamic data from both hydrocodes. By using atomic data from HULLAC, it calculates population dynamics and synthesizes spatially and time resolved x-ray spectra.

The 2D resolved distribution of hydrodynamic parameters ( $\rho_{\text{Al}}$ ,  $\rho_{\text{C}}$  and  $T_e$ ) from the hydrocodes and the intercombination line emission calculated by CRETIN are plotted for five selected simulation times in Fig. 5. The early stage of the primary Al plasma creation is seen at  $t=0$  ns (laser peak maximum). The generation of C plasma induced by impinging Al ions starts before  $t=0.6$  ns and the secondary plasma consisting of both elements expands toward the Al foil during the rest of the simulation. Important information for further discussion is the localization of the emissivity in the final phase,  $t > 1.5$  ns: a prevailing part of the radiation is emitted on the edge of the dense plasma, while the inner volume, closer to the axis of symmetry, radiates less.

The pseudo-2D regime of the hydrodynamic MULTIF simulation does not include radial velocities and therefore the maximal reasonable duration of the simulation is limited, as for later times the absence of the radial plasma expansion becomes significant and the model is less accurate. Since the radial velocities are necessary in the spectral postprocessing to calculate the Doppler shifts, they have been tentatively included into the simulation via parametrization  $v_{\text{rad}}(r,t) = kr/r_{\text{max}}(t-t_0)$ , where  $r$  is the radial position,  $r_{\text{max}} = 240 \mu\text{m}$  is the maximal  $r$  included in the simulation,  $t$  is the time, and  $t_0$  and  $k$  are the free parameters fitted to obtain the best agreement with experimental data. This parametrization presents a very simple but effective way for inclusion of velocities anticipating the cylindrical-like expansion. Its main advantage is that it depends practically on the parameter  $k$  only. The second free parameter  $t_0$  which represents the beginning of the secondary plasma expansion was set to 0.7 ns. The suitability of this parametrization is also supported by the spatial profile of the axial velocity at the end of MULTIF calculation, which is very close to the linear fit  $v_{\text{ax}}(z) = 2.8 \times 10^8 (z - z_{\text{C}})$ , where  $z_{\text{C}}$  is the position of the Carbon foil.

#### 4. Spectra discussion

Profiles of the intercombination line synthesized for three different values of parameter  $k=0, 6, \text{ and } 12 \times 10^{15} \text{ cm s}^{-2}$  are shown in Fig. 6a–c, respectively, and compared with the experimentally observed data (Fig. 6d) extracted from the left-hand side of Fig. 2b. The synthesized line shifts, especially those shown in Fig. 6c, depend on axial position  $z$ , despite the inserted velocity profile is dependent on  $r$  and  $t$  only. This is due to the modeled expansion of the back-scattered plasma. At larger distances of the emitting regions from the C target, the line emission is more delayed. The radial velocity increases with time, thus the delayed emission results in larger Doppler shifts.

Although the agreement between the best-fit simulations and the experimental data is more qualitative than quantitative, the synthesized line profiles clearly identify the Doppler effect as the principal mechanism of the line splitting. The spectral lines do not display any splitting at zero radial velocities (Fig. 6a), whereas with increasing velocities (Fig. 6b and c), the line separation increases. The fit for  $k = 12 \times 10^{15} \text{ cm s}^{-2}$  provides the best agreement to the experimental data. In spectra corresponding to  $z = 300 \mu\text{m}$ , the shift of the side peaks from the line center in both simulation and experiment attains  $\Delta\lambda \approx 4 \text{ m}\text{\AA}$ . This shift implies radial velocity  $v_{\text{rad}} = 1.5 \times 10^7 \text{ cm s}^{-1}$ , which agrees with the maximal axial velocity  $1.7 \times 10^7 \text{ cm s}^{-1}$  present in the MULTIF simulation.

Selected spatially resolved experimentally observed resonance and intercombination line profiles are shown in Fig. 7. These data indicate that the separation of the side peaks starts at  $z \approx 400 \mu\text{m}$  and their shifts related to the central wavelengths (7.757 and 7.807 Å, respectively) increase approximately linearly with the decreasing  $z$  up to  $\Delta\lambda \approx 10 \text{ m}\text{\AA}$  achieved at  $z = 160 \mu\text{m}$ . The side peaks are clearly visible in the intercombination line emission. The side maxima of the resonance line observed in the range of  $z \approx 160\text{--}340 \mu\text{m}$  are present with the same wavelength separation but with a significantly lower intensity.

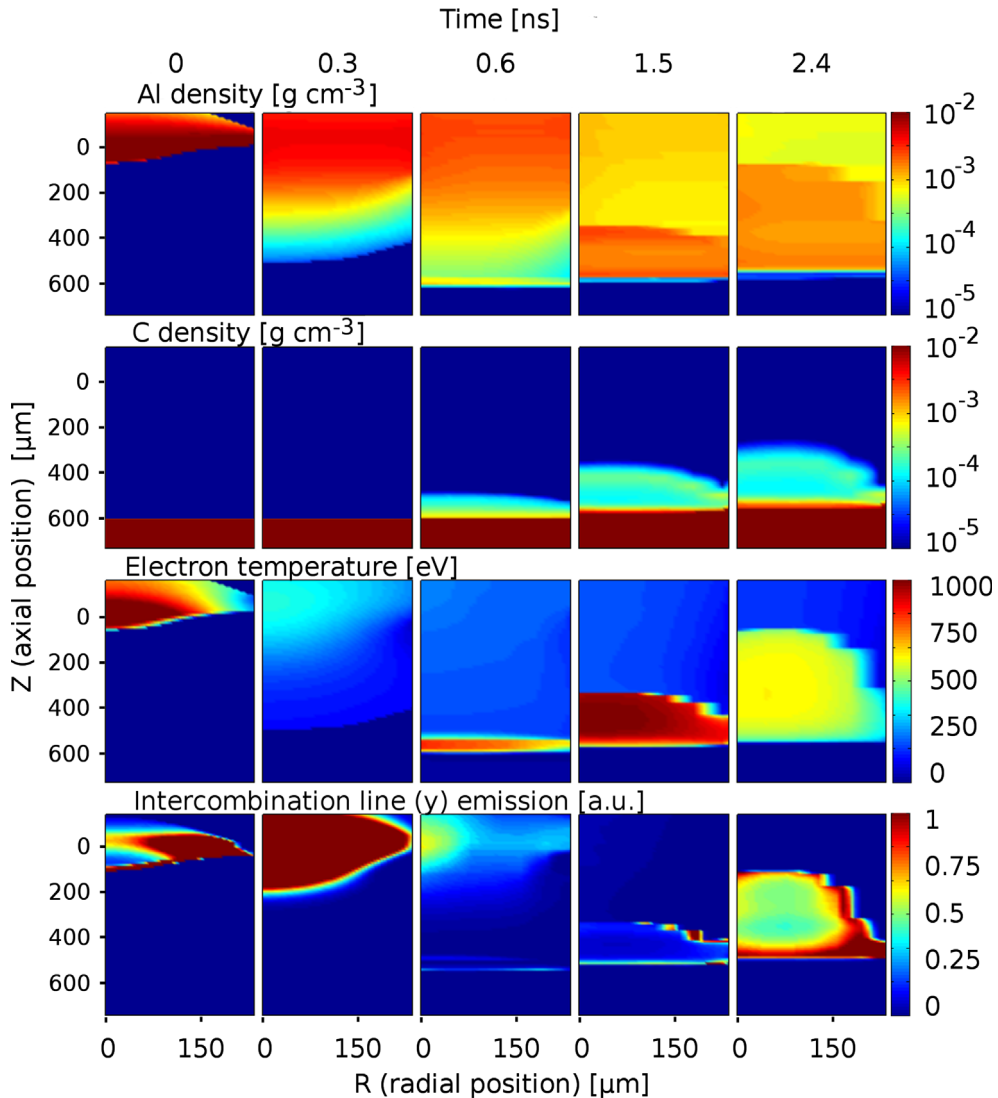


**Fig. 5.** Time evolution of simulated 2D resolved plasma densities, temperature and Al He $\alpha$   $\gamma$  emission. The Al plasma starts to expand before the laser peak maximum ( $t=0$ ) and reaches C target at  $t\approx 0.5$  ns. Afterwards, the mixture of both plasma species is moving backwards. The Al He $\alpha$   $\gamma$  emission attain its maximum during the laser pulse duration but rises again as the reflected plasma starts to cool down.

Both synthetic and experimental spectra exhibit the maximum intensity in the plasma interaction region at  $z=400\text{--}500\ \mu\text{m}$ , i.e., slightly above the C target. In simulations, however, the line wings decay smoothly until their intensity decreases below the intensity of the central peak at  $z\approx 250\ \mu\text{m}$ , whereas the lines experimentally observed in this region undergo an intensity build-up accompanied by an additional increase in the line shifts. This discrepancy between the theory and simulations is explained by approximations used in the spectra modeling. The simulations were performed using the collisional-radiative steady state regime which in principle blocks the non-stationary mechanism of the intercombination line enhancement described in Section 2. The increase of the plasma emission experimentally observed in the range of  $z\approx 200\text{--}300\ \mu\text{m}$  is explained by the capture and accumulation of the back-scattered plasma on the non-ablated cold dense Al.

However, this behavior cannot be verified due to the limited duration of the hydrodynamic simulations. Also the streak camera record (Fig. 3) terminates at  $t=2.6$  ns, i.e., before the expected occurrence of this interaction.

Previous studies of the radially expanding plasmas, see e.g. [10,21] and references therein, proved unambiguously that the profiles of emitted x-ray lines are considerably affected by the macroscopic Doppler shifts. Different plasma elements emitting along the line-of-sight are characterized by mutually shifted absorption and emission profiles, thus producing composite spectral lines with broadened shapes and frequency shifts which reflect the relevant velocity profiles. The distinct splitting of the isolated spectral line is conditioned by an enhanced emission from the expanding plasma surface. As mentioned above, the fulfillment of this condition is demonstrated in Fig. 5 for time 2.4 ns, where the dominant emission is

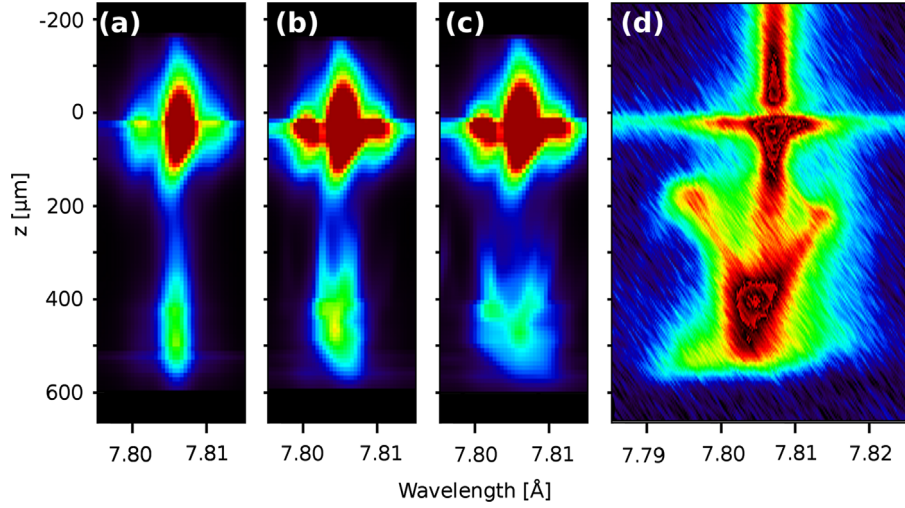


**Fig. 6.** Splitting of the He $\alpha$   $\gamma$  line in the spectra modeled for values of the velocity scaling parameter  $k=0$  (a), 6 (b), and  $12 \times 10^{15} \text{ cm s}^{-2}$  (c) and their comparison with the experimental data (d).

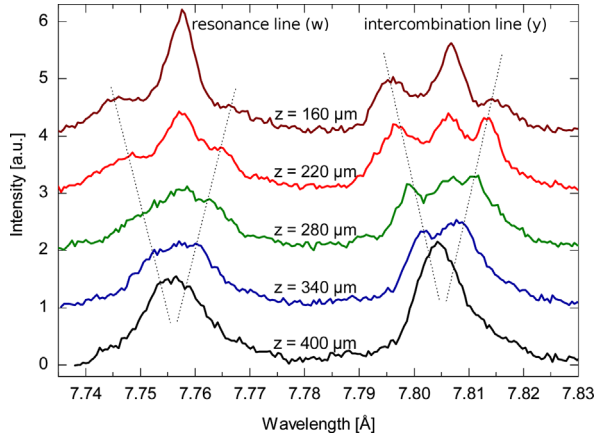


**Fig. 7.** Resonance and intercombination line profiles observed at various positions ( $z$ ) from the rear side of the Al target. The side maxima correspond to the Doppler-shifted emission of the backscattered Al ions. For clarity, the individual profiles were vertically shifted.

localized right on the outer edge of the dense plasma. Due to the highest ion velocity in this outer plasma region, the prevailing part of the emitted radiation is characterized by the highest Doppler shifts thus producing two separate peaks. In contrast, the central part of the spectral line is suppressed due to a weak radiation from the plasma center.

To support this interpretation, a simple analytical model of calculating the modified line profile was constructed. In the chosen cylindrical geometry, the plasma cross-section at the given distance  $z$  is represented by an annulus in the plane perpendicular to the central axis. The dependence of the emissivity on the radius  $\epsilon(r)$  was assumed to be a rectangular function with constant value on a given radii interval ( $r_1, r_2$ ) and zero otherwise. The radial component of the plasma velocity is linearly increasing with the radius  $r$ :  $v_{\text{rad}}(r)=r/r_2 v_{\text{max}}$ . Neglecting the absorption in the plasma, we can write the emergent spectral intensity as  $I(\lambda_0+\Delta\lambda)=k \int \epsilon dV$ , where the integral

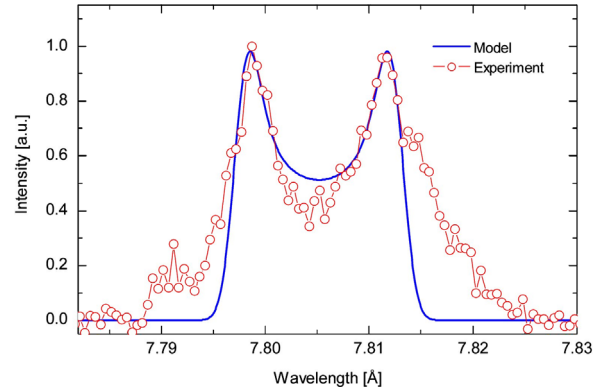


**Fig. 8.** Spectrum of the backscattered plasma obtained by subtracting the profiles measured at single- and double-foil targets for  $z=275 \mu\text{m}$  and its comparison with the line profile modeled for  $v_{\text{max}}=2.8 \times 10^7 \text{ cm s}^{-1}$  and  $a=0.8$ .

goes over the region fulfilling the Doppler condition  $\Delta\lambda=\lambda_0 v_x c^{-1}$ , where  $v_x$  is the velocity component toward the spectrometer,  $c$  the velocity of light,  $\lambda_0$  is the spectral line wavelength, and  $k$  is a constant. Defining the radii ratio  $a$  of the emitting zone  $a=r_1 r_2^{-1}$ , the whole model depends on two parameters only:  $a$  and  $v_{\text{max}}$ .

After the integral was numerically evaluated, the line profile was convolved by a Gaussian peak with FWHM 2.4 mÅ representing the line broadening and the free parameters were optimized. The resulting profile is compared to the experimental data observed at  $z=275 \mu\text{m}$ , see Fig. 8. To obtain the emission only of the plasma backscattered from the C foil, the lineout from the single-foil experiment (Fig. 2a) has been subtracted from the double-foil one (Fig. 2b). The optimal fitting parameters have been found as  $v_{\text{max}}=2.8 \times 10^7 \text{ cm s}^{-1}$  and  $a=0.8$ .

### 5. Conclusion

The impact of laser-produced energetic Al ions onto the secondary C target was investigated using the high-dispersion

spatially-resolving x-ray spectrometer. The observed splitting of the Al He $\alpha$  intercombination line exceeding 15 mÅ was explained by velocity gradients induced Doppler shifts due to the plasma radial expansion.

The interaction scenario has been modeled by multi-fluid pseudo-2D hydrodynamic simulations postprocessed using the collisional-radiative code. The effect of the observed spectral line splitting including the spatial dependence of the wavelength shifts was successfully reproduced in synthetic spectra.

The simulations indicate that the energetic Al ions are decelerated and captured at the C foil where they produce dense Al/C plasma which is back-scattered with the significant radial velocity components. During this backward expansion, the Al He $\alpha$  intercombination line is emitted preferentially on the plasma edge thus enabling to directly observe the radial expansion velocity. This velocity is strongly dependent on the time and position of the emission, its value was estimated to be of the order of  $3 \times 10^7$  cm s $^{-1}$ . A simple analytical model of the line shape formation confirms that the observability of the line splitting depends on the suppression of the emission from the plasma center.

The reported experiment and its detailed theoretical interpretation demonstrate the possibility to visualize the velocity gradients of ions backscattered from the secondary targets thus contributing to the precise spectroscopic investigation of the plasma-wall interaction.

## Acknowledgments

We gratefully acknowledge the help of O. Larroche, M. Busquet and H.A. Scott who provided us an access to their codes, and the assistance of the scientific and technical staff of the PALS research center in performing the experiment. This research has been supported by the Czech Science Foundation, Grant nos. P205/10/0814 and P205/11/0571, by the CTU Grant SGS10/299/OHK4/3T/14 and the MSMT project LM2010014 (PALS Research Infrastructure).

## References

- [1] Remington BA, Drake RP, Ryutov DD. Experimental astrophysics with high power lasers and Z pinches. *Rev Mod Phys* 2006;78: 755–807.
- [2] Bouquet S, Falize E, Michaut C, Gregory CD, Loupiau B, Vinci T, et al. From lasers to the universe: scaling laws in laboratory astrophysics. *High Energy Density Phys* 2010;6:368–80.
- [3] Key MH. Status of and prospects for the fast ignition inertial fusion concept. *Phys Plasmas* 2007;14:055502.
- [4] Honrubia JJ, Fernández JC, Temporal M, Hegelich BM, Meyer-ter-Vehn J. Fast ignition of inertial fusion targets by laser-driven carbon beams. *Phys Plasmas* 2009;16:102701.
- [5] Jacob W, Linsmeier C, Rubel M. 13th international workshop on plasma-facing materials and components for fusion applications. *Phys Scr* 2011;T145:011001.
- [6] Alvarez J, Rivera A, Gonzalez-Arrabal R, Garoz D, del Rio E, Perlado JM. Materials research for HiPER laser fusion facilities: chamber wall, structural material and final optics. *Fusion Sci Technol* 2011;60: 565–9.
- [7] Renner O, Liska R, Rosmej FB. Laser-produced plasma-wall interaction. *Laser Part Beams* 2009;27:725–31.
- [8] Renner O, Rosmej FB, Adámek P, Dalimier E, Delserieys A, Krouský E, et al. Spectroscopic characterization of ion collisions and trapping at laser-irradiated double-foil targets. *High Energy Density Phys* 2007;3:211–7.
- [9] Renner O, Krouský E, Liska R, Šmíd M, Larroche O, Dalimier E, et al. Direct spectroscopic observation of ion deceleration accompanying laser plasma-wall interaction. *J Phys Conf Ser* 2010;244:022024.
- [10] Wark JS, Rose SJ, Patel PK, Djaoui A, Renner O, Hauer A. Astrophysically relevant experiments on radiation transfer through plasmas with large velocity gradients. *Phys Plasmas* 1997;4:2004–10.
- [11] Jungwirth K, Cejnarova A, Juha L, Kralikova L, Krasa J, Krousky E, et al. The prague asterix laser system. *Phys Plasmas* 2001;8: 2495–501.
- [12] Liska R, Limpouch J, Kucharík M, Renner O. Selected laser plasma simulations by ALE method. *J Phys Conf Ser* 2008;112:1–4.
- [13] Renner O, Missalla T, Sondhauss P, Krousky E, Förster E, Chenais-Popovics C, et al. High luminosity, high resolution x-ray spectroscopy of laser produced plasma by vertical geometry Johann spectrometer. *Rev Sci Instrum* 1997;68:2393–403.
- [14] Boiko VA, Chugunov AY, Faenov AYA, Pikuz SA, Skobelev IYu, Vinogradov AV, et al. Anomalous intensity ratios of the resonance to intercombination lines of He-like ions in Nd- and CO $_2$ -laser-produced plasmas. *J Phys B At Mol Phys* 1979;12:213–20.
- [15] Young BKF, Goldstein WH, Osterheld AL, Stewart RE, Charatis G, Busch GE. Spectroscopic analysis of a recombining laser-produced aluminium plasma. *J Phys B At Mol Opt Phys* 1989;22:L533–8.
- [16] Renner O, Adámek P, Angelo P, Dalimier E, Förster E, Krousky E, et al. Spectral line decomposition and frequency shifts in Al He $\alpha$  group emission from laser-produced plasma. *J Quant Spectrosc Radiat Transfer* 2006;99:523–36.
- [17] MacFarlane JJ, Golovkin IE, Wang P, Woodruff PR, Pereyra NA. SPECT3D—a multi-dimensional collisional-radiative code for generating diagnostic signatures based on hydrodynamics and PIC simulation output. *High Energy Density Phys* 2007;3:181–90.
- [18] Chenais-Popovics C, Renaudin P, Rancu O, Gilleron F, Gauthier JC, Larroche O, et al. Kinetic to thermal energy transfer and interpenetration in the collision of laser-produced plasmas. *Phys Plasmas* 1997;4:190–208.
- [19] Klapisch M, Busquet M, Bar-Shalom A. A new and improved version of HULLAC. *AIP Conference Proceedings* 2007;926:206–15.
- [20] Scott HA. Cretin—a radiative transfer capability for laboratory plasmas. *J Quant Spectrosc Radiat Transfer* 2001;71:689–701.
- [21] Irons FE, McWhirter RWP, Peacock NJ. The ion and velocity structure in a laser produced plasma. *J Phys B At Mol Phys* 1972;5:1975–88.